Nature of the Transition between a Ferromagnetic Metal and a Spin-Glass Insulator in Pyrochlore Molybdates

N. Hanasaki,[1,2] K. Watanabe,[1] T. Ohtsuka,[1] I. Kézsmárki,[1,3,4] S. Iguchi,[1] S. Miyasaka,[1,5] and Y. Tokura[1,4,6]

[1]*Department of Applied Physics, University of Tokyo, Tokyo 113-8656, Japan*
[2]*Department of Physics, Okayama University, Okayama 700-8530, Japan*
[3]*Department of Physics, Budapest University of Technology and Economics, 1111 Budapest, Hungary*
[4]*Spin Superstructure Project (SSS), ERATO, Japan Science and Technology Agency, Tsukuba 305-8562, Japan*
[5]*Department of Physics, Osaka University, Toyonaka 560-0043, Japan*
[6]*Correlated Electron Research Center (CERC), National Institute of Advanced Industrial Science and Technology (AIST), Tsukuba 305-8562, Japan*

(Received 29 November 2006; published 21 August 2007)

The metal-insulator transition has been investigated for pyrochlore molybdates $R_2Mo_2O_7$ with nonmagnetic rare-earth ions R. The dynamical scaling analysis of ac susceptibility reveals that the geometrical frustration causes the atomic spin-glass state. The reentrant spin-glass phase exists below the ferromagnetic transition. The electronic specific heat is enhanced as compared to the band calculation result, perhaps due to the orbital fluctuation in the half-metallic ferromagnetic state. The large specific heat is rather reduced upon the transition, likely because the short-range antiferromagnetic fluctuation shrinks the Fermi surface.

DOI: 10.1103/PhysRevLett.99.086401 PACS numbers: 71.30.+h

Metal-insulator transitions are central topics in the field of strongly correlated electron systems [1]. In perovskite manganites $R_{1-x}A_xMnO_3$ (R and A being rare-earth and alkaline-earth ions, respectively), there is strong competition between a ferromagnetic metallic state and an antiferromagnetic charge-orbital ordered state. Such a bicritical phase competition causes a gigantic response to external stimuli [2]. The quenched disorder due to the size difference of R^{3+} and A^{2+} ions tends to suppress or extinguish the long-range charge-orbital order [3]. In the region where the long-range order is absent, an atomic spin-glass state is caused by spin frustration due to the disorder of the site potential and interaction [4]. A similar transition between a spin-glass state and a ferromagnetic state was also reported for the pyrochlore molybdates [5–7]. The geometrical frustration of the pyrochlore lattice even with a constant antiferromagnetic interaction may give rise to anomalous spin states such as the spin liquid state [8–10]. In the metal-insulator transition of the pyrochlore molybdates, where the phase competition (bicriticality) and geometrical frustration are both at work, the interplay between the spin state and the charge transport is of particular interest. Furthermore, because of the orbital degeneracy within the t_{2g} levels of Mo^{4+} ions, the orbital degree of the freedom may remain active, as well. The purpose of this study is to investigate the metal-insulator transition and its relevance to Mo spin structures for $R_2Mo_2O_7$ with nonmagnetic R ions.

In the pyrochlore molybdates $R_2Mo_2O_7$, the trigonal crystal field divides the Mo $4d$ t_{2g} manifold into a lower a_{1g} level and higher degenerate e_g' levels [5,11,12]. Since the Mo atom is nominally tetravalent, one electron exists in the a_{1g} level and the other occupies the e_g' level, which contributes to the charge transport. For the larger R-ion radius r_R, the Mo-O-Mo angle is large, leading to the ferromagnetic half-metallic state [5,13]. The orbital degrees of the freedom remain active, whereas the spin degrees of the freedom are essentially quenched. For the smaller r_R, antiferromagnetic interaction is favored, leading to the spin-glass insulating state caused by geometrical frustration. The optical spectra revealed the disappearance of the Drude weight and the continuous growth of the Mott gap, on reducing the R-ion radius [14–16]. Recent transport measurements have revealed the continuous Mott-Anderson transition [17], in contrast with the canonical first-order Mott transition [18,19].

All the pyrochlore molybdates reported so far have the magnetic R sites with large moments, which unfortunately cover the intrinsic nature of the magnetization and the electronic heat capacity inherent to the Mo sites with their large contribution to these quantities. In this Letter, we report the magnetic properties and the heat capacity for pyrochlore molybdates with no magnetic moment on the R site. $Eu_2Mo_2O_7$ is located on the verge of the Mott transition. By substituting the Eu site with nonmagnetic Y or La, we could change the average R-ion radius as a control parameter of the phase transition.

The sintered polycrystalline samples of $(Eu_{1-x}Y_x)_2Mo_2O_7$ and $(Eu_{1-y}La_y)_2Mo_2O_7$ were prepared by reacting Eu_2O_3, Y_2O_3, La_2O_3, and MoO_2. Single crystals of $Eu_2Mo_2O_7$ were obtained by a floating zone method. The magnetization, heat capacity, resistivity, and Seebeck coefficient were measured by quantum design physical property measurement system.

The main panel of Fig. 1(a) shows the temperature dependence of magnetization in $(Eu_{1-x}Y_x)_2Mo_2O_7$ and

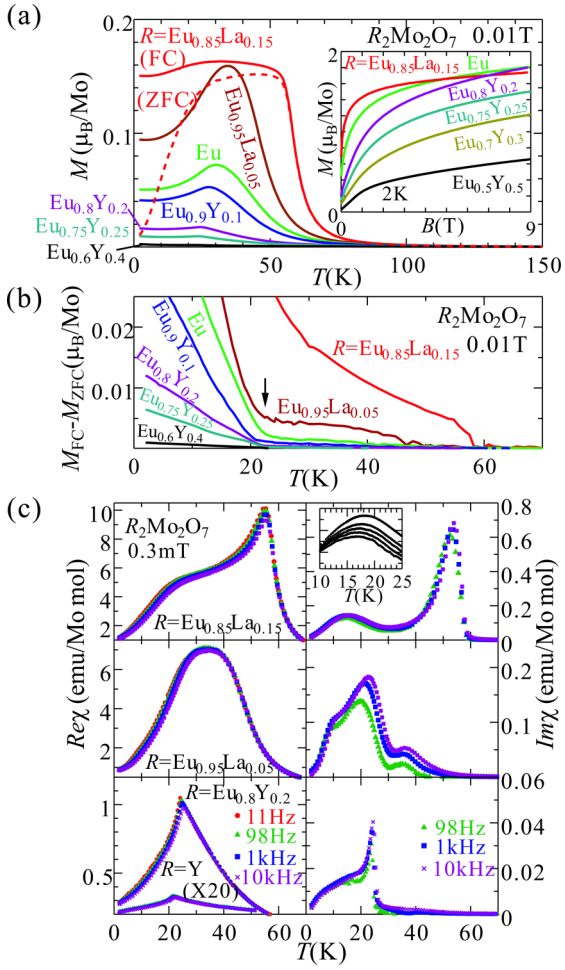

FIG. 1 (color online). (a) Magnetization measured in field cooling (0.01 T) in $(Eu_{1-x}Y_x)_2Mo_2O_7$ ($x = 0.1$, 0.2, 0.25, and 0.4) and $(Eu_{1-y}La_y)_2Mo_2O_7$ ($y = 0$, 0.05, and 0.15). The broken curve shows the magnetization of $(Eu_{0.85}La_{0.15})_2Mo_2O_7$ measured in 0.01 T after the zero-field cooling. Inset: magnetization up to 9 T at 2 K. (b) Difference in the magnetization between the field cooling and the zero-field cooling. (c) The ac magnetic susceptibility {in-phase [Reχ] (left panel) and out-of-phase component [Imχ] (right panel)} measured by 0.3 mT at 11 (●), 98 (▲), 1 k (■) and 10 kHz (×) in $(Eu_{1-x}Y_x)_2Mo_2O_7$ ($x =$ 0.2 and 1) and $(Eu_{1-y}La_y)_2Mo_2O_7$ ($y = 0.05$ and 0.15). Inset: Imχ near the reentrant transition (from top to bottom; 3.3 k, 1 k, 333, 98, and 31 Hz).

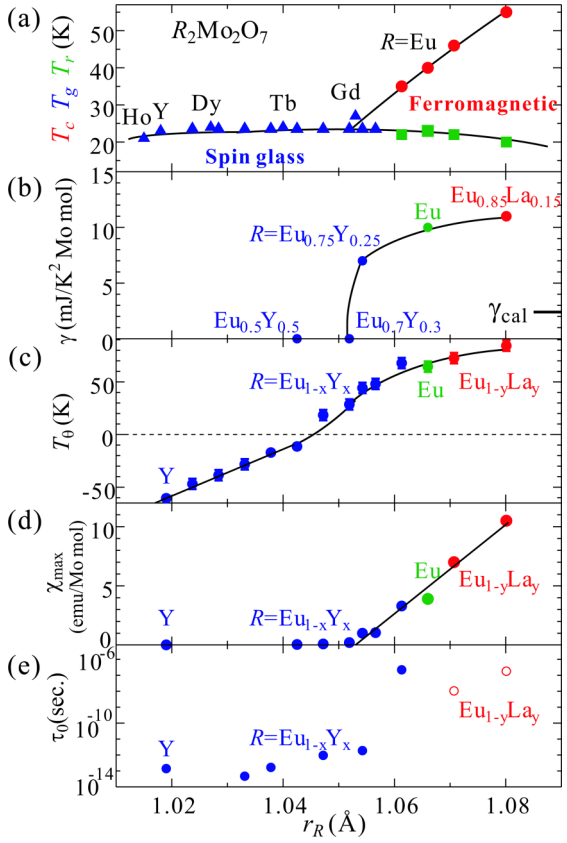

FIG. 2 (color online). The R-site ionic radius (r_R) dependence of various quantities in $R_2Mo_2O_7$. (a) Temperature of the ferromagnetic transition (T_c, ●), the spin-glass transition (T_g, ▲), and the reentrant transition (T_r, ■) of $(Eu_{1-x}Y_x)_2Mo_2O_7$, $(Eu_{1-y}La_y)_2Mo_2O_7$, and the end materials $R_2Mo_2O_7$. (b) Electronic specific heat γ. The right-hand horizontal bar indicates the electronic specific heat γ_{cal} derived from the band calculation [5]. (c) Weiss temperature T_θ. (d) Maximum value χ_{max} of the ac magnetic susceptibility with variation of temperature. (e) Flipping time τ_0 in the logarithmic expression, which was estimated by the dynamical scaling of the ac susceptibility. The closed circles and the open ones are calculated by the in-phase and the out-of-phase susceptibility, respectively. Solid lines in (a)–(d) are merely the guide to the eyes.

$(Eu_{1-y}La_y)_2Mo_2O_7$. The substitution of Eu with La enlarges the averaged R-site ionic radius (r_R), which increases the electron transport and favors the ferromagnetic interaction. The $(Eu_{0.85}La_{0.15})_2Mo_2O_7$ undergoes the ferromagnetic transition at $T_c = 56$ K. As depicted in the inset, the magnetization increases without a discontinuity in applying the magnetic field, and it was nearly saturated at $M_{sat} \approx 1.7\mu_B$ in the high magnetic field, which is comparable to the Mo moment value ($\approx 1.4\mu_B$) estimated by neutron scattering measurements [11,20]. As displayed in Fig. 2(c), the Weiss temperature is positive ($T_\theta = 85$ K) at $r_R \approx 1.08$ Å, suggesting the dominance of ferromagnetic double-exchange interaction.

In $Y_2Mo_2O_7$, the magnetic susceptibility anomaly shows a cusplike structure, as presented in the lower panel of Fig. 1(c) [10,21]. The antiferromagnetic interaction is stabilized owing to the small R-site radius and leading to the spin-glass state on the frustrated pyrochlore lattice. This is consistent with the negative Weiss temperature ($T_\theta = -61$ K), as depicted in Fig. 2(c). Figure 3(a) displays the detailed frequency dependence of the magnetic susceptibility. We performed the dynamical scaling analysis with the inverse of frequency f as the observation time τ. We found the scaling relation between the reduced temperature $\epsilon = (T_f - T_g)/T_g$ and τ, as shown in the inset. Here, T_f and T_g denote the peak temperature measured at the frequency f and the transition temperature in the low frequency limit, respectively. We obtained the critical exponents $z\nu = 7.7$, with $T_g = 20.8$ K and the

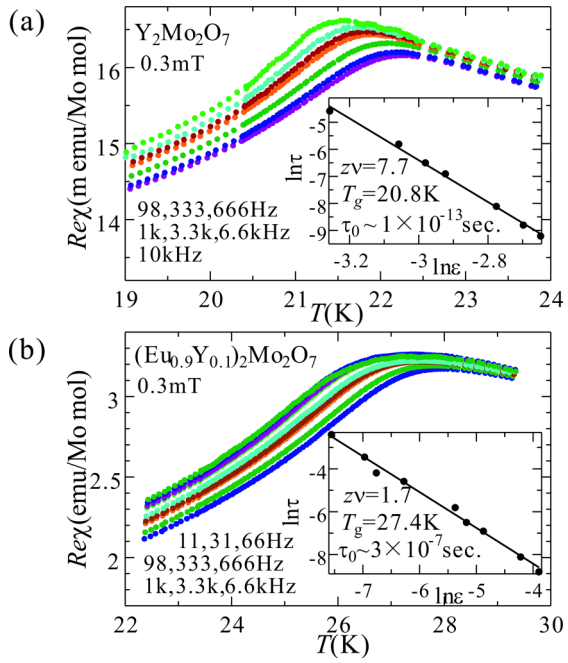

FIG. 3 (color online). (a) The in-phase ac magnetic susceptibility (from top to bottom; 98, 333, 666 Hz, 1 k, 3.3 k, 6.6 k, and 10 kHz) measured by 0.3 mT in $Y_2Mo_2O_7$. Inset: dynamical scaling of the observation time τ with the reduced temperature $\epsilon = [T_f - T_g]/T_g$. (b) The in-phase ac magnetic susceptibility (from top to bottom; 11, 31, 66, 98, 333, 666 Hz, 1 k, 3.3 k, and 6.6 kHz) in $(Eu_{0.9}Y_{0.1})_2Mo_2O_7$. Inset: dynamical scaling of τ with ϵ.

spin flipping time $\tau_0 \sim 1 \times 10^{-13}$ sec, according to the scaling relation, $\tau/\tau_0 = [(T_f - T_g)/T_g]^{-z\nu}$ [4]. Here, z and ν denote the dynamical critical exponent and the critical exponent of the spin correlation length, respectively. This short flipping time τ_0 indicates the nature typical of *atomic-scale* spin-glass state caused by the geometrical frustration [4].

The difference in the magnetization between the field cooling (FC) and the zero-field cooling (ZFC) process is given in Fig. 1(b). In $(Eu_{0.85}La_{0.15})_2Mo_2O_7$, this difference appears at the ferromagnetic transition temperature (T_c = 56 K). As shown in the upper panel of Fig. 1(c), there is another frequency-dependent shoulderlike anomaly around $T_r \approx 20$ K. The magnetization under ZFC is suppressed below T_r, suggesting the reentrant spin-glass phase. We performed the dynamical scaling analysis with use of the temperature of the maximum in the out-of-phase susceptibility Imχ in the region of a shoulderlike anomaly in Reχ [22]. This analysis gives the critical exponents $z\nu = 3.5$, and the spin flipping time $\tau_0 \sim 2 \times 10^{-7}$ sec. This long flipping time suggests that the reentrant phase is a spin-glass state, in which the ferromagnetic cluster is randomly oriented. The determination of T_r in the reentrant case is not as accurate as in the spin-glass case [22].

Figure 2(a) displays the variation of the ferromagnetic (T_c), the spin glass (T_g), and the reentrant (T_r) transition temperatures with the R-site ionic radius r_R. Here, T_c and T_r are defined as the temperature at which the difference (M_{FC}-M_{ZFC}) appears in the magnetization between FC and ZFC, and the temperature at which the difference M_{FC}-M_{ZFC} shows an additional upturn, as indicated by an arrow in Fig. 1(b), respectively. In reducing r_R, the T_c decreases, converges to the T_r at $r_R \approx 1.055$ Å, and they connect to the T_g. The Weiss temperature also decreases and changes its sign around $r_R \approx 1.05$ Å, as shown in Fig. 2(c). In general, the magnetic susceptibility diverges at the ferromagnetic transition, while it remains finite at the spin-glass transition. Thus, one can expect a discontinuity in the maximum value of the susceptibility at the transition. Nevertheless, the maximum value changes continuously in the transition region, as depicted in Fig. 2(d). We also present the change of the spin flipping time τ_0 versus r_R in Fig. 2(e). The flipping time ($\tau_0 \sim 10^{-13}$ sec) remains typical of a microscopic relaxation time at $r_R \leq 1.055$ Å [4]. With increasing r_R, the ferromagnetic cluster is expected to grow in size. In accord with this expectation, the spin flipping time τ_0 is enhanced up to $\tau_0 \sim 3 \times 10^{-7}$ sec at $r_R \approx 1.06$ Å, suggesting the crossover to the spin-glass state with the ferromagnetic cluster.

Let us discuss the metal-insulator transition controlled by r_R. Figure 4(a) shows the Seebeck coefficient S. For the larger averaged-r_R compounds (R = Eu and $Eu_{0.85}La_{0.15}$), the Seebeck coefficient approaches zero at the low temperature, suggesting the metallic ground state. By contrast, it diverges for the smaller averaged-r_R compounds (R = $Eu_{0.75}Y_{0.25}$ and $Eu_{0.5}Y_{0.5}$) in the insulating ground state. The temperature dependence of S for the insulating ground-state compounds is unusually nonmonotonic, reminiscent of the thermal crossover from insulator to metal. According to the optical study [14,15], the thermally induced closing of the charge gap is observed to form the high-temperature incoherent conduction state in accord with the thermoelectrics. The inset depicts the resistivity of the sintered samples. In $R = Eu_{0.85}La_{0.15}$, which is located nominally in the metallic phase region, the resistivity tends to increase with lowering the temperature perhaps due to Anderson localization effect. In accord with the reduction in transfer energy with the Y content (x) in $(Eu_{1-x}Y_x)_2Mo_2O_7$, the low-temperature resistivity increases for $x \geq 0.2$, suggesting the opening of the charge gap.

The temperature dependence of heat capacity in B = 0 T and 9 T in $Eu_2Mo_2O_7$ is given in the inset of Fig. 4(b). The heat capacity in $B = 0$ T contains the contribution of spin excitation or magnons [23]. In order to remove this contribution by enlarging the magnon gap, we measured the heat capacity in a magnetic field. The main panel shows the C/T versus T^2 plot at $B = 9$ T. The electronic specific heat γ can be estimated by the extrapolation toward zero temperature as shown by the broken lines, although the nuclear Schottky component still remains at the lowest temperature. Figure 2(b) depicts the r_R dependence of the heat capacity. The density of states deduced from the

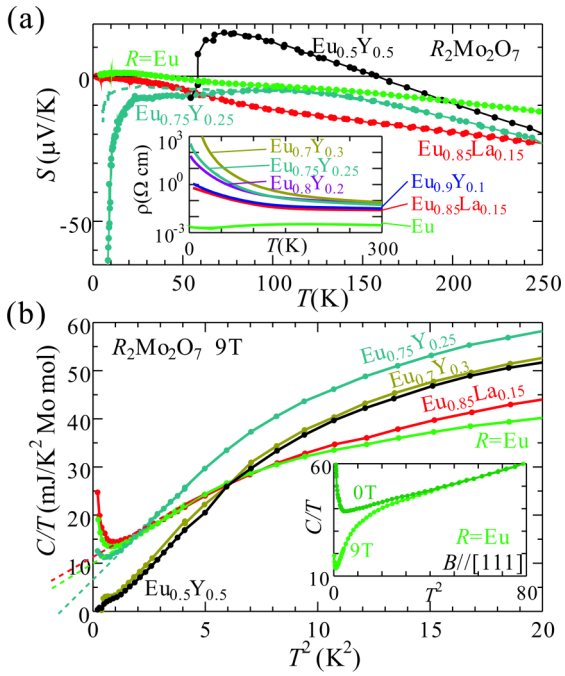

FIG. 4 (color online). (a) Temperature dependence of the Seebeck coefficient S of $(Eu_{0.85}La_{0.15})_2Mo_2O_7$ and $(Eu_{1-x}Y_x)_2Mo_2O_7$ ($x = 0$, 0.25, and 0.5). The broken curve indicates the Seebeck effect at 9 T in $(Eu_{0.75}Y_{0.25})_2Mo_2O_7$. Inset: temperature dependence of the resistivity in the single crystal $Eu_2Mo_2O_7$ (bottom) and the sintered polycrystalline samples $(Eu_{0.85}La_{0.15})_2Mo_2O_7$ and $(Eu_{1-x}Y_x)_2Mo_2O_7$ [$x =$ 0.1, 0.2, 0.25, and 0.3 (top)]. (b) Temperature dependence of the specific heat measured in 9 T for $(Eu_{0.85}La_{0.15})_2Mo_2O_7$ and $(Eu_{1-x}Y_x)_2Mo_2O_7$ ($x = 0$, 0.25, 0.3, and 0.5). Broken lines indicate the extrapolation toward zero temperature. Inset: specific heat of $Eu_2Mo_2O_7$ measured in 0 T and 9 T.

band calculation for the pyrochlore molybdates gives the electronic specific heat coefficient $\gamma_{\rm cal} \approx 2.4$ mJ/K^2 mol [5], as indicated by the horizontal bar on the right ordinate. Since the measured $\gamma(= 11$ mJ/K^2 mol) is much larger than that of the band calculation, the effective mass of the conduction electron appears strongly renormalized. In such an almost half-metallic state, however, the mass renormalization by the spin fluctuation should not work, and hence the orbital degree of freedom is the only remaining factor. As a possible origin of the mass enhancement, we may consider the orbital fluctuation of the conduction electrons in the e_g/ band of the t_{2g} manifold [5], such as orbital analogy of antiferromagnetic fluctuation.

As r_R decreases, the electronic heat capacity is reduced and approaches zero near $r_R \approx 1.052$ Å. The saturated value of magnetization starts to decrease as r_R becomes smaller than $r_R \approx 1.054$ Å ($(Eu_{0.75}Y_{0.25})_2Mo_2O_7$). The spin flipping time is also shortened, suggesting the transition from the reentrant spin-glass state with the ferromagnetic cluster to the atomic spin-glass state. The antiferromagnetic interaction between the neighboring sites becomes dominant and finally leads to the insulating spin-glass state, which is anticipated to grow in the reentrant spin-glass state. This short-range antiferromagnetic fluctuation may cause the shrinkage of the Fermi surface, leading to the reduction of the γ [24]. In $r_R \approx 1.054$ Å ($(Eu_{0.75}Y_{0.25})_2Mo_2O_7$), the observed insulatorlike Seebeck effect reveals that the states residing at the Fermi level, as suggested by a finite value of the electronic specific heat, cannot contribute to the carrier conduction owing perhaps to the Anderson localization.

In summary, the geometrical frustration causes the *atomic* spin-glass state on the insulating side of the phase diagram, while the reentrant spin-glass state exists below ferromagnetic transition on the metallic side. The effective electron mass, which is enhanced perhaps via the orbital degree of freedom in the half-metallic ferromagnetic state, is reduced upon the transition owing to the short-range antiferromagnetic fluctuation.

We thank Y. Taguchi, K. Sano, M. Imada, R. Mathieu, N. Nagaosa, and S. Onoda for discussions. This work was supported by Grants in Aid for Scientific Research (No. 15740202, No. 17340104, No. 19014015, and No. 19540341) from MEXT, the Bolyai János research program, and the Hungarian Scientific Research Fund Grant (No. F61413).

[1] M. Imada *et al.*, Rev. Mod. Phys. **70**, 1039 (1998).
[2] Y. Tokura, Rep. Prog. Phys. **69**, 797 (2006).
[3] Y. Tomioka and Y. Tokura, Phys. Rev. B **70**, 014432 (2004).
[4] R. Mathieu *et al.*, Phys. Rev. Lett. **93**, 227202 (2004).
[5] I. V. Solovyev, Phys. Rev. B **67**, 174406 (2003).
[6] T. Katsufuji *et al.*, Phys. Rev. Lett. **84**, 1998 (2000).
[7] Y. Taguchi *et al.*, Phys. Rev. B **65**, 115102 (2002).
[8] Y. Shimizu *et al.*, Phys. Rev. Lett. **91**, 107001 (2003).
[9] S. T. Bramwell and M. J. P. Gingras, Science **294**, 1495 (2001).
[10] J. S. Gardner *et al.*, Phys. Rev. Lett. **83**, 211 (1999).
[11] Y. Taguchi *et al.*, Science **291**, 2573 (2001).
[12] H. Ishikawa *et al.*, Phys. Rev. B **70**, 104103 (2004).
[13] Y. Moritomo *et al.*, Phys. Rev. B **63**, 144425 (2001).
[14] I. Kézsmárki *et al.*, Phys. Rev. Lett. **93**, 266401 (2004).
[15] I. Kézsmárki *et al.*, Phys. Rev. B **73**, 125122 (2006).
[16] M. W. Kim *et al.*, Phys. Rev. Lett. **92**, 027202 (2004).
[17] N. Hanasaki *et al.*, Phys. Rev. Lett. **96**, 116403 (2006).
[18] P. Limelette *et al.*, Science **302**, 89 (2003).
[19] F. Kagawa *et al.*, Nature (London) **436**, 534 (2005).
[20] Y. Yasui *et al.*, J. Phys. Soc. Jpn. **72**, 865 (2003).
[21] J. L. Tholence, Solid State Commun. **35**, 113 (1980).
[22] K. Jonason *et al.*, Phys. Rev. B **53**, 6507 (1996).
[23] R. Konno and T. Moriya, J. Phys. Soc. Jpn. **56**, 3270 (1987).
[24] S. Miyasaka *et al.*, J. Phys. Soc. Jpn. **69**, 3166 (2000).